

DTIC FILE COPY

WRDC-TR-90-2059

AD-A223 033



ELECTROSTATIC FUEL ATOMIZATION AND SPRAY  
DISPERSAL DEMONSTRATION

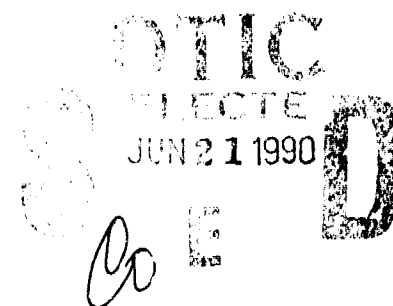
A.J. Kelly

ZYW Corporation  
P.O. Box 279  
Princeton Junction, NJ 08550

July 1990

Final Report for Period September 1989 - January 1990

Approved for Public Release; Distribution is Unlimited



AERO PROPULSION AND POWER LABORATORY  
WRIGHT RESEARCH AND DEVELOPMENT CENTER  
AIR FORCE SYSTEMS COMMAND  
WRIGHT-PATTERSON AIR FORCE BASE, OHIO 45433-6563

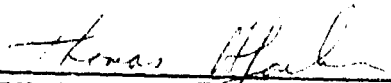
90 06 20 054

# NOTICE

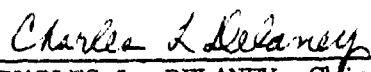
When Government drawings, specifications, or other data are used for any purpose other than in connection with a definitely Government-related procurement, the United States Government incurs no responsibility or any obligation whatsoever. The fact that the government may have formulated or in any way supplied the said drawings, specifications, or other data, is not to be regarded by implication, or otherwise in any manner construed, as licensing the holder, or any other person or corporation; or as conveying any rights or permission to manufacture, use, or sell any patented invention that may in any way be related thereto.

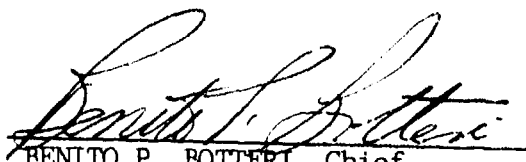
This report is releasable to the National Technical Information Service (NTIS). At NTIS, it will be available to the general public, including foreign nations.

This technical report has been reviewed and is approved for publication.

  
THOMAS A. JACKSON, Project Engineer  
Fuels Branch  
Fuels and Lubrication Division  
Aero Propulsion and Power Laboratory

FOR THE COMMANDER

  
CHARLES L. DELANEY, Chief  
Fuels Branch  
Fuels and Lubrication Division  
Aero Propulsion and Power Laboratory

  
BENITO P. BOTTERI, Chief  
Fuels and Lubrication Division  
Aero Propulsion and Power Laboratory

If your address has changed, if you wish to be removed from our mailing list, or if the addressee is no longer employed by your organization please notify WRDC/POSE, WPAFB, OH 45433-6563 to help us maintain a current mailing list.

Copies of this report should not be returned unless return is required by security considerations, contractual obligations, or notice on a specific document.

UNCLASSIFIED

SECURITY CLASSIFICATION OF THIS PAGE

## REPORT DOCUMENTATION PAGE

Form Approved  
OMB No 0704-0188

1a. REPORT SECURITY CLASSIFICATION <b>Unclassified</b>		1b. RESTRICTIVE MARKINGS	
2a. SECURITY CLASSIFICATION AUTHORITY		3. DISTRIBUTION/AVAILABILITY OF REPORT Approved for public release; distribution is unlimited	
2b. DECLASSIFICATION/DOWNGRADING SCHEDULE		5. MONITORING ORGANIZATION REPORT NUMBER(S) WRDC-TR-90-2059	
4. PERFORMING ORGANIZATION REPORT NUMBER(S) ZYW-0001Z		7a. NAME OF MONITORING ORGANIZATION Aero Propulsion & Power Laboratory (WRDC/POSF) Wright Research & Development Center	
6a. NAME OF PERFORMING ORGANIZATION ZYW Corporation	6b. OFFICE SYMBOL (if applicable) WRDC/POSF	7b. ADDRESS (City, State, and ZIP Code) Wright Patterson AFB OH 45433-6563	
6c. ADDRESS (City, State, and ZIP Code) P. O. Box 279 Princeton Junction NJ 08550	9. PROCUREMENT INSTRUMENT IDENTIFICATION NUMBER F33615-89-C-2937		
8a. NAME OF FUNDING/SPONSORING ORGANIZATION Fuels Branch, Fuels & Lubrication Division	8b. OFFICE SYMBOL (if applicable) WRDC/POSF	10. SOURCE OF FUNDING NUMBERS	
8c. ADDRESS (City, State, and ZIP Code) Wright-Patterson AFB OH 45433-6563		PROGRAM ELEMENT NO. 65502F	PROJECT NO. 3005
		TASK NO. 21	WORK UNIT ACCESSION NO. 49
11. TITLE (Include Security Classification) ELECTROSTATIC FUEL ATOMIZATION & SPRAY DISPERSAL DEMONSTRATION			
12. PERSONAL AUTHOR(S) A. J. Kelly			
13a. TYPE OF REPORT Final	13b. TIME COVERED FROM Sep 89 TO Jan 90	14. DATE OF REPORT (Year, Month, Day) 1990 July	15. PAGE COUNT 36
16. SUPPLEMENTARY NOTATION			
17. COSATI CODES		18. SUBJECT TERMS (Continue on reverse if necessary and identify by block number)	
FIELD	GROUP	SUB-GROUP	
21	04		
21	02		
		electrostatic atomization, spraying, fuel, charged droplets, plume, self-dispersal, droplet distribution	
19. ABSTRACT (Continue on reverse if necessary and identify by block number)			
<p>The purpose of this work is to characterize charged spray plumes, test the validity of existing spray/plume models, provide a basis for evaluating these plumes for gas turbine fuel and ignitor systems service. Plumes generated by a charge injection atomizer in nitrogen (≤6 bar, absolute) have been analyzed using an Aerometrics Phase Doppler Particle Analyzer (PDPA). A 10 bar pressure test chamber suitable for use with charged sprays and with the PDPA was designed and fabricated. A two regime plume structure is confirmed. At 1 bar the outer, "small droplet" sheath is characterized by a Sauter mean diameter (<math>D_{32}</math>) of <math>\approx 55\mu\text{m}</math>, a span of <math>\approx 0.7</math> and a number median of <math>\approx 20\mu\text{m}</math>. The inner, "large droplet" core is characterized by <math>D_{32} \approx 110\mu\text{m}</math> and the same span. These data conform to a predicted overall droplet size distribution exhibiting a polydispersed profile: primary peak at <math>\approx 105\mu\text{m}</math>, and secondary peaks at <math>\approx 85</math> and <math>135\mu\text{m}</math>. The peaks are associated with the core region; the near constant.</p>			
20. DISTRIBUTION/AVAILABILITY OF ABSTRACT <input checked="" type="checkbox"/> UNCLASSIFIED/UNLIMITED <input type="checkbox"/> SAME AS RPT. <input type="checkbox"/> DTIC USERS		21. ABSTRACT SECURITY CLASSIFICATION UNCLASSIFIED	
22a. NAME OF RESPONSIBLE INDIVIDUAL I. A. JACKSON		22b. TELEPHONE (Include Area Code) (513) 255-6462	22c. OFFICE SYMBOL WRDC/POSF

DD Form 1473, JUN 86

Previous editions are obsolete.

SECURITY CLASSIFICATION OF THIS PAGE  
UNCLASSIFIED

Block 19. (Continued)

profile below  $\sim 85\mu\text{m}$  is characteristic of the sheath. Contrary to prediction,  $D_3$  increased modestly with pressure in these tests due to two factors: output charge density levels remained fixed with increasing pressure due to shortening of the sprayer caused by droplets stagnating in the test chamber; and, the predicatable, lateral plume core expansion to the probe sampling position. A modest air flow over the spray unit corrects these problems.

The charge plume exhibits vigorous self-dispersivity and has droplet sizes that are suitable for gas turbine fuel systems. These plumes should be beneficial for ignitor systems, particularly for the difficult conditions that exist during altitude relight. In addition, the characteristics of charge injected spray plumes should be of interest for other fuel system uses and for non-combustion uses such as coatings and agricultural spraying.

Accession For	
NIIS GRA&I	<input checked="" type="checkbox"/>
DTIC TAB	<input type="checkbox"/>
Unannounced	<input type="checkbox"/>
Justification	
By	
Distribution/	
Availability Codes	
Available for	



A-1

---

## I. PURPOSE of the WORK

The primary technical objective of the effort is the characterization of electrically charged spray plumes in order to:

- a. provide a data base to test the validity of existing isolated, single plume models.
- b. evaluate the utility of charged electrostatic spray plumes for gas turbine ignition and primary fuel delivery systems.
- c. establish the features of all such plumes.

### Overview Of Electrostatic Atomization:

Almost without exception, all liquid fuels are in droplet form at sometime during the combustion process. Consequently, the control of the atomization process is an essential prerequisite for the achievement of optimal combustion. Ideally, the atomization process ought to permit the detailed manipulation of spray patternation and droplet size distribution to provide precise spatial and/or temporal placement of the incoming fuel. This has proven to be difficult to achieve using conventional spray technology. Such systems, as exemplified by the air blast atomizer, involve the use of aerodynamic forces for droplet development and dispersal and to a greater or less degree, are all constrained by the global fluid dynamics of the engine. As a result, existing systems offer few options that would permit the independent control of droplet generation, plume patternation, and fuel distribution in the combustion zone.

Electrostatic atomization does not rely upon conventional aerodynamic effects, but instead involves the long range electrostatic repulsive force for droplet development and dispersal.

This process inherently circumvents the limitations of existing systems and provides a range of options unavailable from any spray technology not involving free charge. Although electrostatic atomization has been described in the technical literature for a quarter of a millennium, it is only with the advent of the SPRAY TRIODE® atomizer (1), (2) that the application of charged spraying to fuel systems has become a realistic option. The theoretical and technological development work of the past 16 years (3-10) has demonstrated that it is possible to exercise control of the atomization process by purely electrical means and to do this independent of the general fluid mechanical aspects of the fuel delivery process. The prospect now exists for tailoring the atomization process for optimal combustion.

Droplet surface charge is the one factor that uniquely distinguishes electrostatic sprays from all others. Neglecting, for the moment, the equally novel characteristics of charge injection atomizers, it is the presence of free charge and the associated long-range electrostatic force that provide new dimensions in the spray plume parameter space. As a result, the behavior of electrostatic sprays (and sprayers) is sufficiently different from all other means of droplet generation and dispersal as to constitute a major study area. Despite some recent work (11-17), this is an area that has not been the subject of the methodical evaluation and validation.

### Technical Background:

It is now well established that free charge is the sine qua non of all electrostatic atomization.

Equally well established is the remarkable fact that, for technically important fluids (e.g. viscosity below 200 cp) and technically interesting sprays (droplet size  $\geq 1\mu\text{m}$ ), mean droplet size will be determined solely by the free charge density of the fluid. It is this fact, first recognized in the mid 70s, (4) that led directly to the concept of direct charge injection atomization (1). While there are several ways that excess free charge can be introduced into a fluid, the simplest, most rugged and compact means is the SPRAY TRIODE® atomizer. In this device, exemplified by the test device shown in cross section in Figure I-1, two submerged electrodes form a self-contained field emission electron gun assembly.

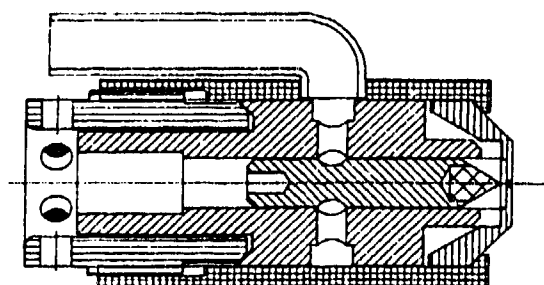


Figure I-1

The centrally located emitter electrode is positioned immediately upstream of a grounded orifice through which the fluid to be atomized exits. If no voltage is applied to the emitter, the fluid simply issues from the orifice, orifices, slit or slits (depending on the design) without disruption. However, if negative voltage is applied to the emitter then free excess charge is driven into the exiting fluid. The charged fluid, once free of the confines of the device, automatically atomizes. In many respects, the device functions much the same as a Van de Graaff generator. Modest input voltages ( $\approx 10$  kV), permit the injection of small amounts of free charge. Only  $4\mu\text{A/mL}$  ( $4\text{ C/m}^3$ ) is all that is necessary for vigorous atomization and the development of very high space charge elec-

tric fields (10 to 20 MV/m is typical). It is the presence of this space charge field that drives the charged droplets outward from the atomizer; aerodynamic or fluid dynamic forces are not involved and are not needed. This is a purely electrodynamic effect.

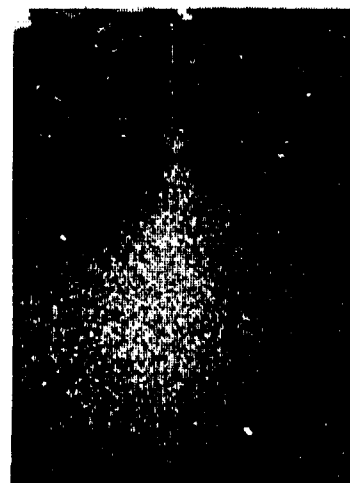


Figure I-2

The photograph of Figure I-2, depicts a 0.91 mL/s Jet-A spray plume in atmospheric air, generated by  $\approx 12\text{ mW}$  of input electrical power to a 1/4 mm circular orifice SPRAY TRIODE® device. In the absence of this electrical input, the spray collapses and reverts to a simple column, characteristic of flow through a circular orifice.

A large data base has been developed since the first proof of concept tests were conducted in October of 1976. This work has shown that the SPRAY TRIODE® atomizer can provide an array of attributes that are unavailable from conventional spray systems. In addition to the aforementioned intense droplet dispersivity in dense gas, we now know that these devices are capable of providing:

- Almost monodisperse droplet size distributions,
- Energetically efficient droplet development,

*-Mean droplet size in the 10 to 100 micron range, insensitive to flow rate and fluid properties, and uniquely related to injected charge density level.*

Of equal or perhaps more importance, from an engineering standpoint, the SPRAY TRIODE® atomizer and the electrostatic spray process are the only spray device (8,9) and spray phenomenon (3-5) for which quantitative, predictive, first principles models exist.

Comparison of the predictions of these models with the limited droplet size distribution data obtained at atmospheric conditions using Malvern droplet sizer and holographic techniques show that they are accurate to within about 20%. It is now possible to calculate the fundamental properties of all SPRAY TRIODE® sprays, without the use of free constants, once the device dimensions and general operating conditions are specified.

This modeling capability is illustrated by the plots of Figures I-3 to I-6. These plots display the manner in which the spray droplet size distribution from a 254  $\mu\text{m}$ , (10 mil) diameter orifice atomizer varies as the background pressure of room temperature air is increased from nominal atmospheric conditions (Figure I-3) to the limiting 4.4 atmosphere level of Figure I-6. Further pressure increase does not influence the droplet formation process. A "best fit" continuous Rosin-Rammler distribution has been overlaid on the calculated histograms for comparison purposes. While the charged spray plume distributions are only approximately represented by the empirical Rosin-Rammler curve the comparison is useful as a means to illustrate that SPRAY TRIODE® spray droplet size distributions are inherently narrower than those of conventionally generated, non-electrostatic sprays. Even the broadest droplet size distribution, which is

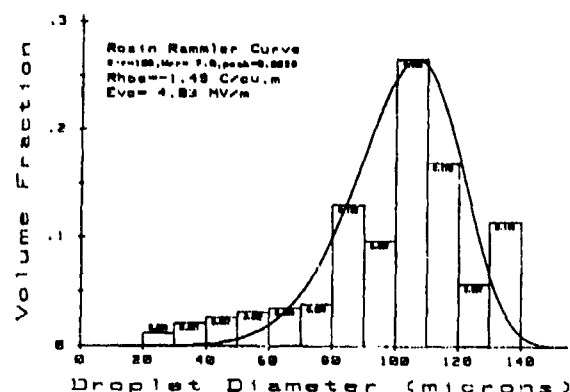


Figure I-3 - 1 bar absolute

associated with atmospheric conditions (cf Figure I-3) has a width parameter that is over twice that of a well designed and constructed conventional atomizer. In other words, the charged spray droplet size span is less than half that of the conventional device.

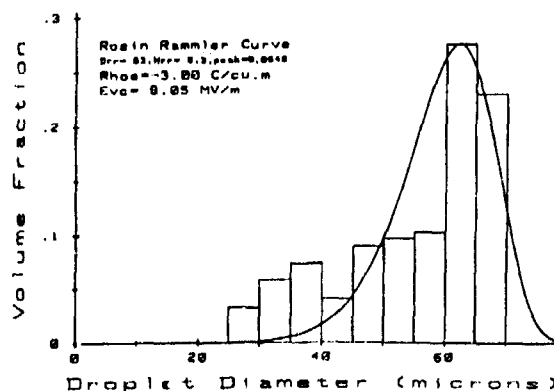


Figure I-4 - 2.4 bar absolute

Increasing background pressure serves to monotonically restrict this droplet size span. Both the larger droplet and the smaller droplet populations are diminished with increasing pressure. This is an intrinsic feature of charge injection atomizers that serves both to sharpen the distribution and to shift the distribution peak to successively smaller values. The large droplet tail, characteristic of conventional sprays, is absent.

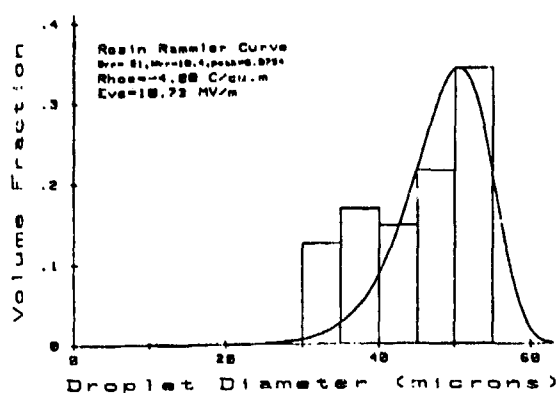


Figure I-5 - 3 bar absolute

The ultimate result of this behavior is displayed in Figure I-6, which indicates that all droplet plumes in 4.4 atmosphere air, and higher, will be constrained in a seven micron interval between 35 and 42 microns. The crudely approximate Rosin-Rammler distribution shown on this plot has a peak at 38 microns and a width parameter of 17.7, a level commensurate with the almost monodisperse nature of this spray.

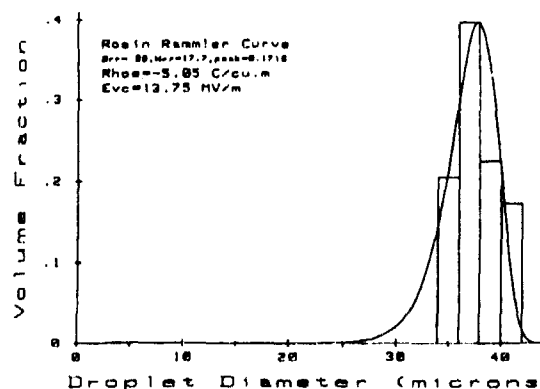


Figure I-6 - 4.4 bar absolute

Important as it is for the development of combustion models this singular capability nevertheless represents only half of what is ultimately required. Despite simplifying assumptions and a preoccupation with single plumes generated by circular orifices, M. True's plume model, (15) published in 1983, and the work of Bellan, (16) and Harstad and Bellan

(11) are the only meaningful models now available to fill this gap in our computational repertoire. Even though the initial conditions, the essential physics and the descriptive equations are now available, today we still do not have available a working description of charged plumes from a generalized single aperture, let alone the multiple aperture arrays that are required for the flow rates typical of gas turbine engine nozzles.

An example of the output from True's plume model is shown in Figure I-7. Using the 38 micron peak droplet size of Figure I-6, as being representative of the plume generated by a 254  $\mu\text{m}$ , (10 mil) SPRAY TRIODE® atomizer operating in a five atmosphere background pressure, the plot illustrates plume

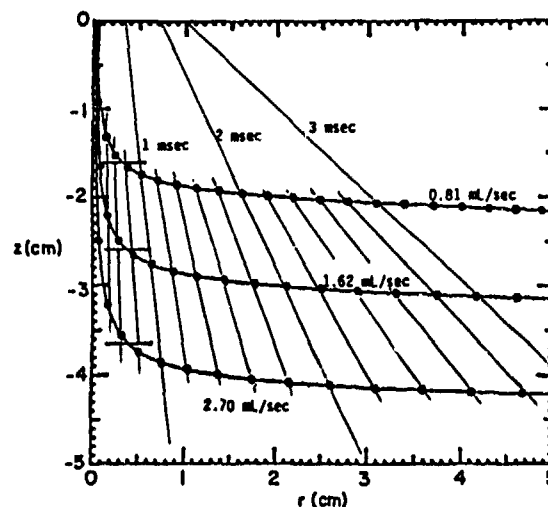


Figure I-7

patternation behavior for various flow rates. The curves represent the plume boundary with the interior of the plume having a uniform droplet population. A general feature, predicted for all SPRAY TRIODE® plumes, is the increase of the lateral dispersal velocity with flow rate. At a flow rate of 0.81 mL/sec, the plume is predicted to expand at a rate of about 10 m/sec. By contrast, a three fold increase in



flow rate to 2.70 mL/sec through the same device produces a plume expansion velocity of 20 m/sec. This behavior is related to the Van de Graaff generator effect. With increasing fluid flow rate, the self generated space charge electric field acts to retard the plume forward motion and to accelerate the droplets radially. By simply adjusting the flow rate and the orifice pattern, it is possible to tailor the plume geometry.

Another feature of this plume is worth noting. Even if the spray is polydisperse, all of the droplets, will behave in essentially the same manner in response to the plume electric field. This unique characteristic of electrostatic spray plumes is due to a fortuitous balance of electrostatic and viscous drag forces; a balance that is insensitive to droplet size. It is straightforward to show that under general conditions the outwardly directed electrostatic force experienced by a droplet due to the space charge electric field is directly related to droplet diameter. The only restraining force encountered by the droplet, that due to viscous drag, at the low Reynold's numbers associated with the velocities in these plumes, (order of 102) is also directly related to droplet diameter and is only weakly dependent upon gas density. Consequently, droplet dispersion will proceed in the same manner for all droplets in the spray, independent of size. Moreover, the dispersion will not be meaningfully altered by gas pressure. Only gas viscosity will be a strong determinant of plume behavior. Despite the obvious utility of these characteristics for cold or altitude start ignition sprays or for tailoring fuel air ratios no data are available to test the validity of these calculations.

## II. DESCRIPTION of the WORK

The available plume patternation data (cf reference 2) were obtained using Malvern droplet sizing and holographic measurement techniques. Neither of these techniques provide droplet velocity data, and neither yield information on spatial variation of droplet size distribution within the plume. To overcome these short comings, the Aerometrics Phase Doppler Analyzer (PDPA) (17-19) was selected to be the primary diagnostic tool for this study. As will be discussed in the Results section, the highly localized nature of the Aerometrics PDPA data makes it difficult to compare these data with the global, integrated distribution data generated by the Malvern droplet sizer and with the calculated droplet size distributions such as those shown in Figures I-3 to I-6. Nevertheless, it is the localized PDPA data that will ultimately be of most use in designing fuel ignition and atomization systems based on SPRAY TRIODE® technology.

In addition to the Aerometrics PDPA, the experimental apparatus used for all testing consists of: a test chamber; the spray device; and a computerized atomizer power supply, fluid supply, data collection and control system. A brief description of each of these test system components follows.

### The Test Chamber:

The test chamber design has been defined by three general criteria;

- a. capability for operation to 10 bar,
- b. compatibility with the Aerometrics PDPA spray measurement system,

c. ability to accommodate the vigorously self-dispersive plumes produced by SPRAY TRIODE® devices in close proximity to the optical access ports.

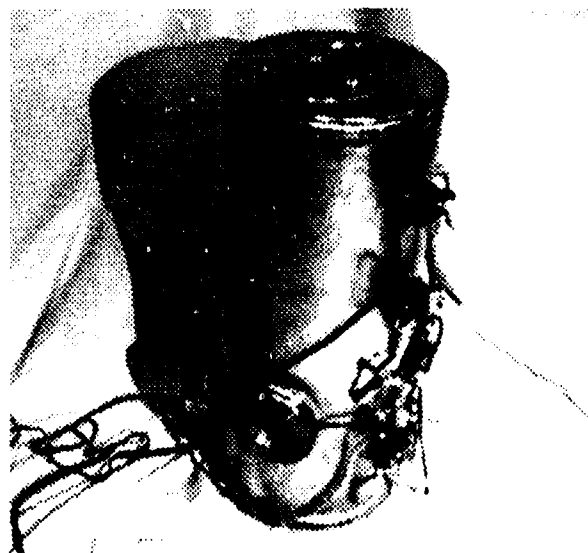


Figure II-1

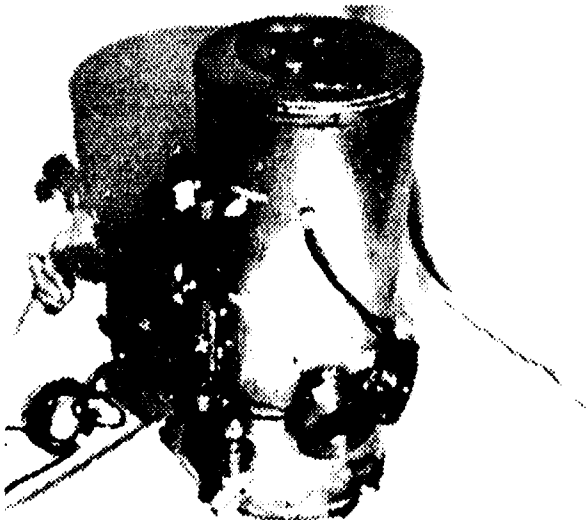


Figure II-2

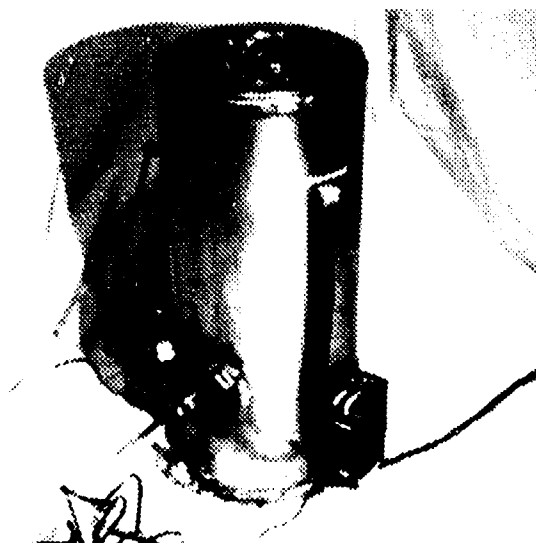
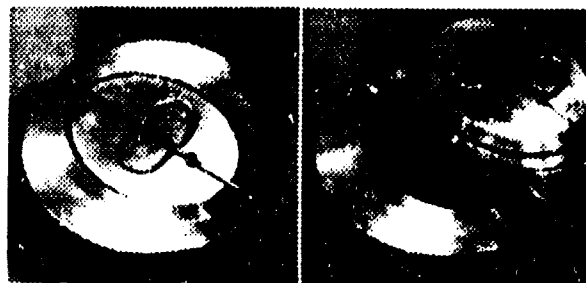


Figure II-3

These three general criteria have been incorporated into, and have defined, the chamber design. Figures II-1 through 3 show different exterior views of the completed test chamber. The chamber is approximately half meter in height with an outside diameter of 20 cm and a 17 1/2 cm inside diameter. Optical access is via three 5 cm diameter by  $\approx 13$  mm thick optical flats two of which are diametrically positioned with the axis 14 cm above the interior base closure plane. The third port, which is displaced radially by  $45^\circ$  from the other two at the same vertical position, permits the determination of radial droplet velocities.

To facilitate testing, and to eliminate sealing



Figures II-4,5

problems typically encountered with flanged end closure designs, an elliptical closure port design has been used. Close up photographs of this closure port are shown in Figure II-4 (closed) and II-5 (open). Design drawings of these parts and the other critical elements of the chamber design are contained in Appendix A. The elliptical end port design has proven to be convenient and easy to use. The somewhat restricted access it provides to the interior, as compared to a conventional flanged closure, has not been an issue of any significance. As shown in Figure II-5, a single "O" ring serves to seat the port to the upper surface with the "P" shaped pins being used to restrain the port in place during initial pressurization. Once seated under pressure, the pins can be returned to their retracted position.

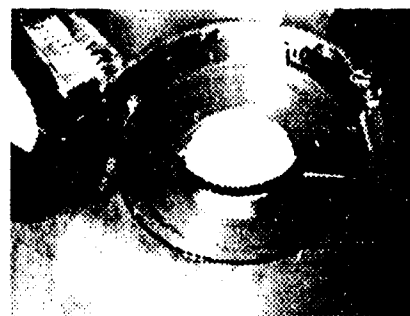


Figure II-6



Figure II-7

The viewports, shown in the photographs of Figures II-6 and 7 and in the detailed engineering drawings of Appendix A, were designed to serve several purposes. First and foremost, the ports have to provide as wide an interior viewing angle as possible to permit maximum flexi-

bility with respect to the placement of the input and exiting probe beams. As a result, the port length has been reduced to the absolute minimum necessary to accommodate the optical flats without having them protrude into the interior. This requirement is established by the second design feature; the need for rapid removal for cleaning during operation at pressure. As noted previously, the intensely dispersive nature of charged sprays produces almost immediate fouling of surfaces in the vicinity of the spray, whether these surfaces are the conductive metal chamber walls or the insulating Pyrex viewports. Experience has shown that the only way to circumvent this problem is to physically shutter the viewports, opening the shutters only during data collection, and then having available a convenient means to remove and clean the ports once they have become fouled.

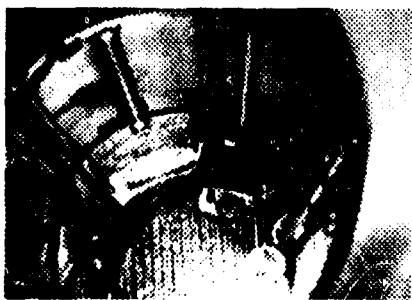


Figure II-8

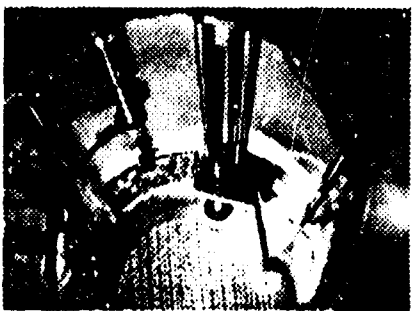


Figure II-9

The shutters, shown in the interior view photographs of Figures II-8 (the single port shutter open) and II-9 (port in the closed position), not only shield the port windows from the spray, but are designed to seal off the ports from the chamber as well. While in the closed position,

the shutters permit the gas between the shutter and the viewport to be vented and the port to be removed. The short neck design serves to facilitate rapid venting of the shutter/viewport volume, with the split retainer ring design shown in Figure II-6, permitting rapid port removal. In the closed position, the retainer rings force the optical flats inward against the canted lip seal that can be seen as the black annular ring in the right part of Figure II-7. A thin (1 1/2 mm) elastomer ring on both sides of the optical flats, as can be seen in the left port in the photograph of Figure II-7, and more clearly in Figure II-10, serves to assist sealing to the lip seal and to cushion the outward surface where it presses against the split retainer rings. Once the port/shutter volume is vented the split rings can be safely removed and the port removed using the suction cup

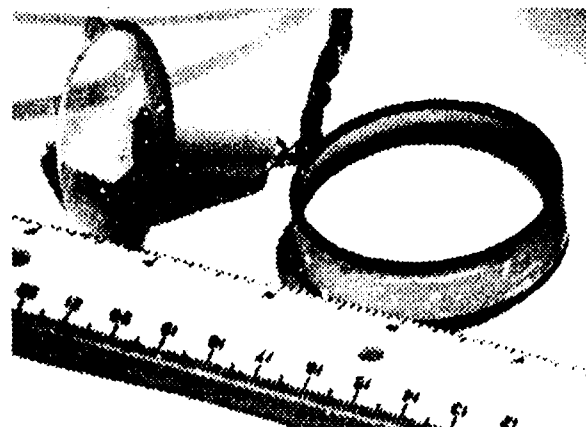


Figure II-10



Figure II-11

shown in Figure II-10 and in use in Figure II-11. Typically, the window interior surface is cleaned while it remains attached to the removal unit facilitating rapid replacement and the resumption of testing.



Figure II-12

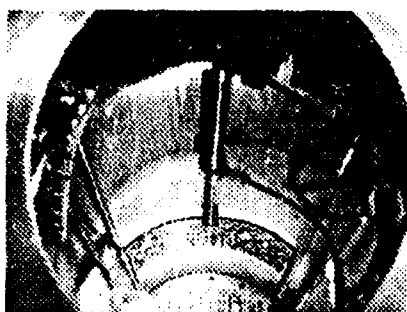


Figure II-13

As shown in the interior views of Figures II-8,9, and 12-15 the interior has a free standing structure consisting of an upper annular ring and eleven vertical rods. The upper ring supports the shutter system, with the rods acting to guide the dual port shutter shown in Figures II-12 (open) and 13 (closed) and as a guide way and motor mount support for the SPRAY TRIODE® traversing system that can be seen in Figures II-8 and 9. Both shutters are simply mounted on dual acting pneumatic cylinders, which are secured to the cage ring. Actuation is provided by external solenoid control, as is port venting. These solenoid valves can be seen in the overall exterior views of Figures II-1 and 2.

The SPRAY TRIODE® traversing mechanism

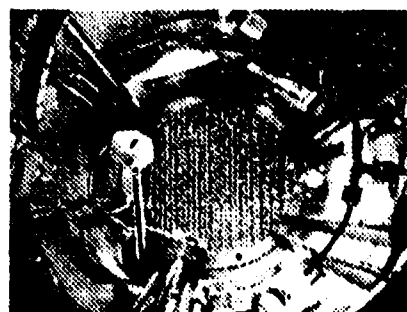


Figure II-14

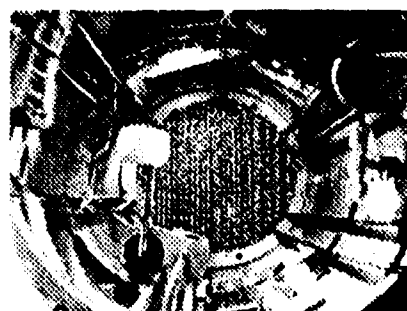


Figure II-15

(cf Figures II-8,9 and Figures II-14 and 15) has been designed to permit remote control of vertical and radial position of the spray device and presetting of the angular orientation of the spray axis with the chamber axis. This latter feature is illustrated in the photographs of Figures II-14 and 15 where the SPRAY TRIODE® mount is oriented parallel to the chamber axis in Figure II-14 and is canted by 30° in Figure II-15. In this canted position the spray plume can be probed along a fixed radial angle as the sprayer vertical position is varied. The Delrin SPRAY TRIODE® mount has been designed to accommodate 16 mm diameter devices or, with a Teflon adapter, 10 mm Series 18 devices. In both instances, the spray unit is electrically isolated from the support arm permitting the interelectrode current to be monitored. As shown in Figure II-16, the orifices of both units have the same radial position with respect to the radial traverse motor shaft. The shaft length has been selected to permit the orifice to be placed directly on the centerline of the chamber if needed. This geometry is preferred if the SPRAY TRIODE® is

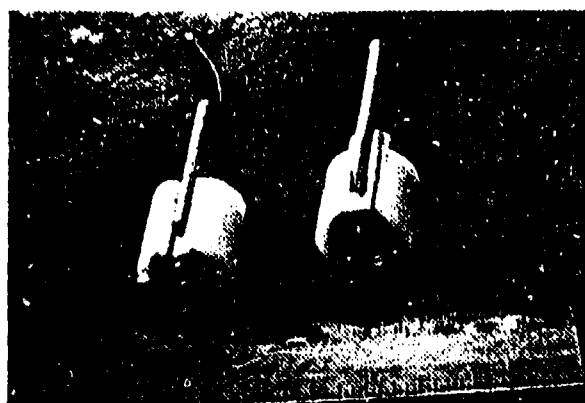


Figure II-16

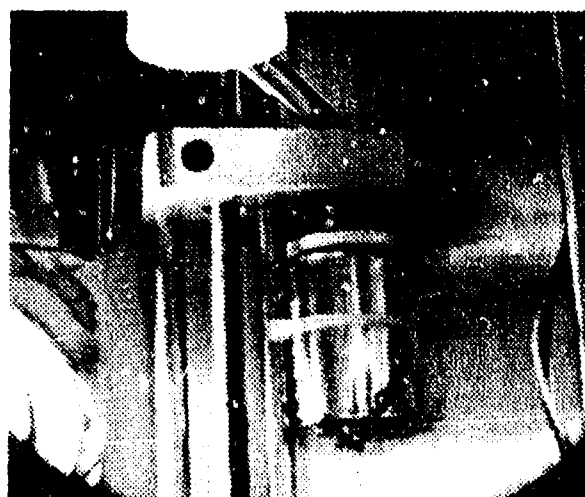


Figure II-17

detached from the radial traverse motor and is hard mounted to the vertical traverse plate by insertion into the mating hole that is clearly seen in Figure II-17. Rigid mounting is desirable when angular traverses (the spray and chamber axis are skew) are being made. The same type of geared DC (12V) motor is used for both the radial traverse and the vertical translation. To avoid the possibility of motor burnout, should the vertical limits of the screw driven mount be inadvertently exceeded, the drive screw is connected to the motor shaft by a soft copper shear pin (cf Figure II-18). Motor speed has been selected to provide a vertical traverse velocity of  $1 \text{ mm/sec} \pm 4\%$ .

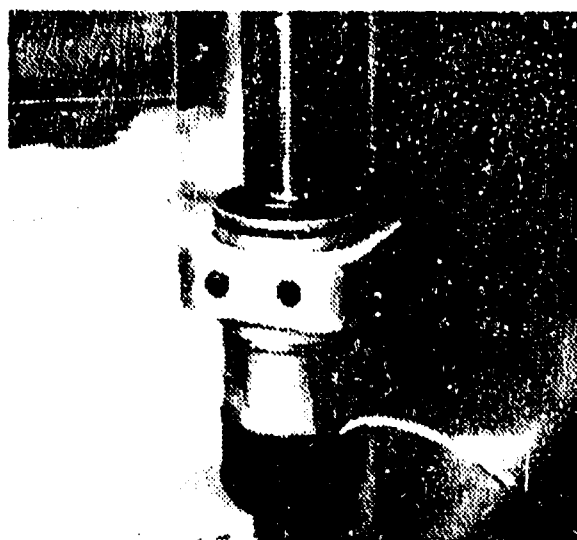


Figure II-18

Except for manual venting, all chamber functions are handled via the control box shown in Figure II-19. The box is powered by 110V AC,

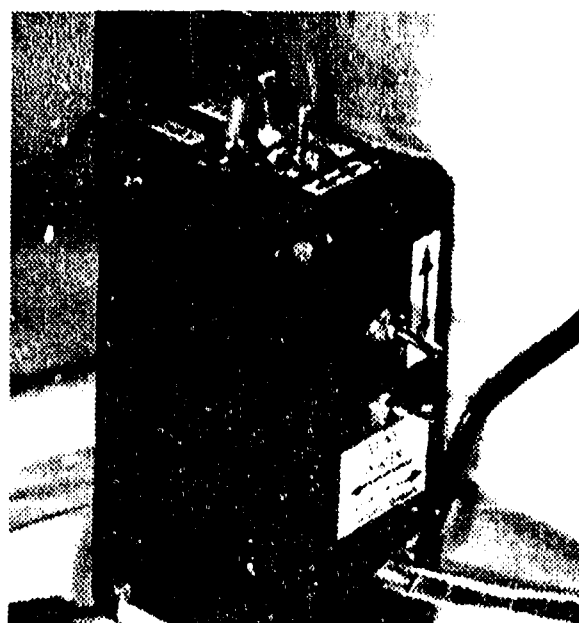


Figure II-19

used by the solenoid valves, and by 12V DC, which is converted to accommodate the different speed requirements of the vertical and radial traversing motors. The center-off switches, designated by arrows, permit trav-

erse control. The side mounted vent switch actuates the port vent solenoid. As a safety feature this switch is interlocked with the two shutter control switches seen on the control box top surface adjacent to the radial traverse switch. The simple on/off shutter control switch closest to the chamber actuates the shutter cylinder solenoid valves to open the normally (zero input power) closed shutters. When this switch is off, the light colored switch next to it can be used to momentarily open the shutter, which remains open as long as the switch is manually actuated. Inactivation of these switches, when the ports are vented, prevents opening of the shutters and the possibility of an explosive expulsion of unsecured window ports during the window cleaning operation.

Another safety feature, not seen in the view of Figure II-19, is a neon lamp that is mounted on the far side of the control box. The 90 V neon bulb is hard wired between the chamber and a permanently connected ground lead. This prevents dangerous levels of charge build up from occurring should the spray current ( $I_c$ ) lead connected from the chamber to the spray current meter inadvertently be disconnected. It is worth noting that all electrical circuitry has been designed to assure isolation from the chamber, which, in turn, is electrically isolated from its surroundings in order to permit the direct reading of total collected spray current. Spray fluid and pressurizing gas for the shutters and the chamber are introduced via 1/8" ( $\approx 3$  mm) nylon tubing. In all instances, nitrogen is used as a safety measure to obviate the possibility of combustible mixture formation. Aluminum filter matting is placed on the bottom of the chamber as a sparge, spatter and froth suppression barrier, cf Figures II-8,9 and II-12 to II-18. Collected spray fluid is manually vented and either drains by gravity during atmospheric tests or is expelled by chamber pressure during operation at elevated pressures.

### SPRAY TRIODE® Test System:

The computer (HP-9816) controlled pumping station used for all open SPRAY TRIODE® testing and data collection, is described in the schematic of Figure II-20. This unit, which is

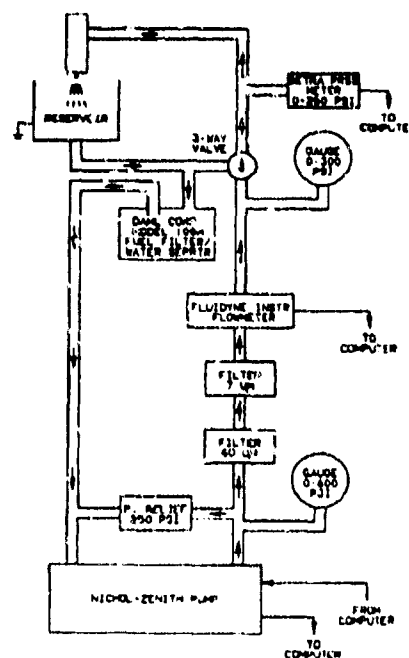


Figure II-20

an integral part of the overall test system shown in the photograph of Figure II-21, permits independent computerized control of both the flow rate ( $Q$ ) and the high voltage input ( $V_c$ ) to the SPRAY TRIODE® unit and the



Figure II-21

periodic collection of data. The data are automatically collected for detailed analysis on floppy disc, and can be printed out on command whenever a "real time" hard copy is necessary. As displayed in the printout sheet of Figure II-22, in addition to pumping system related data such as flow rate, pump speed, and input pressure ( $P_h$ ), the printout also lists fluid temperature ( $T_f$ ), chamber pressure ( $P_c$ ) and

```

STIB007A 30 Jan 1990 CHARACTERIZATION TESTS:7024 CAL FLUID
Data Index Number = 440
Time = 15:56:17 Elapsed Time = 451 sec

Nichols-Tenish Reading----- 150
Head Pressure, (Ph)----- 140 (kPa), 20.3 (Psi)
Chamber Pressure, (Pc)----- 101 (kPa), 14.6 (Psi)
Flow Rate, (Q)----- .88 (ml/sec)
Fluid Temp, (Tf)----- 1.0 (deg C)
Input Voltage, (Vi)----- -9.12 (kV)
Spray Current, (Is)----- -1.42 (micro-amp)
Blunt Electrode Current, (Ib)----- -1.97 (micro-amp)
Blunt Electrode Voltage, (Vb)----- -.09 (kV)
Inter-electrode Voltage, (Va-Vb)----- -9.03 (kV)
Total Current, (Ia+Ib)----- -3.39 (micro-amp)
Total Electrical Power, (VaIa)----- 30.90 (mW)
Spray Power, (VsIs)----- 13.0 (mW)
Total Input Power, (VaIa + PHEU)----- 150.4 (mW)
Mean Charge Density, (Ic/Q)----- -1.67 (C/cu.m.)

STIB007A 30 Jan 1990 CHARACTERIZATION TESTS:7024 CAL FLUID
Data Index Number = 440
Time = 15:57:07 Elapsed Time = 472 sec

Nichols-Tenish Reading----- 150
Head Pressure, (Ph)----- 136 (kPa), 19.8 (Psi)
Chamber Pressure, (Pc)----- 101 (kPa), 14.6 (Psi)
Flow Rate, (Q)----- .84 (ml/sec)
Fluid Temp, (Tf)----- 1.3 (deg C)
Input Voltage, (Vi)----- -8.67 (kV)
Spray Current, (Is)----- -1.38 (micro-amp)
Blunt Electrode Current, (Ib)----- -1.78 (micro-amp)
Blunt Electrode Voltage, (Vb)----- -.08 (kV)
Inter-electrode Voltage, (Va-Vb)----- -8.59 (kV)
Total Current, (Ia+Ib)----- -3.16 (micro-amp)
Total Electrical Power, (VaIa)----- 27.14 (mW)
Spray Power, (VsIs)----- 12.0 (mW)
Total Input Power, (VaIa + PHEU)----- 142.3 (mW)
Mean Charge Density, (Ic/Q)----- -1.64 (C/cu.m.)

STIB007A 30 Jan 1990 CHARACTERIZATION TESTS:7024 CAL FLUID
Data Index Number = 475
Time = 15:57:18 Elapsed Time = 482 sec

Nichols-Tenish Reading----- 150
Head Pressure, (Ph)----- 135 (kPa), 19.5 (Psi)
Chamber Pressure, (Pc)----- 101 (kPa), 14.6 (Psi)
Flow Rate, (Q)----- .84 (ml/sec)
Fluid Temp, (Tf)----- 1.3 (deg C)
Input Voltage, (Vi)----- -8.67 (kV)
Spray Current, (Is)----- -1.36 (micro-amp)
Blunt Electrode Current, (Ib)----- -1.73 (micro-amp)
Blunt Electrode Voltage, (Vb)----- -.08 (kV)
Inter-electrode Voltage, (Va-Vb)----- -8.60 (kV)
Total Current, (Ia+Ib)----- -3.09 (micro-amp)
Total Electrical Power, (VaIa)----- 26.83 (mW)
Spray Power, (VsIs)----- 11.8 (mW)
Total Input Power, (VaIa + PHEU)----- 139.6 (mW)
Mean Charge Density, (Ic/Q)----- -1.63 (C/cu.m.)

```

Figure II-22

SPRAY TRIODE® electrical parameters. These include operating voltage ( $V_i$ ) supplied by the computer controlled Bertan 205A-20N high voltage power supply, and the spray ( $I_s$ ) and interelectrode ( $I_b$ ) currents measured by Keithley model 480 picoammeters. For convenience, the printout also lists a variety of derived quantities such as the blunt electrode voltage, interelectrode voltage, total current, total electrical power, spray power, and total

(hydraulic plus electrical) input power and the mean output charge density level ( $I_c/Q$ ). As noted on the printout, each suite of data has a detailed label, is dated, and has both the absolute time plus the relative time of collection with respect to the start of the data collection sequence. Data can be collected at preselected time intervals of one second or longer. The data sequence number is also provided as an indexing tool. Previous work with the Aerometrics PDPA system has shown that the most useful way to correlate the SPRAY TRIODE® test system data with the droplet distribution data, is to synchronize the clocks of the two systems to within  $\approx 15$  seconds, and to use the absolute time line as the primary means to correlate the two data sets.

#### The SPRAY TRIODE® Atomizer:

Although, a four orifice test unit was fabricated and was available for testing, for reasons that will be explained, all data were obtained using a single orifice Series 18 device. This device is the 10 mm diameter device shown to the left of the 16 mm diameter, 4 orifice unit depicted in the photograph of Figure II-16 and is shown in the cross-sectional drawing of Figure I-1. The particular device used for all testing has a single 254  $\mu\text{m}$  diameter orifice and no swirl. Without applied voltage, the stream is smooth and unperturbed. The data printouts of Figure II-22 displays a typical data sequence during operation, in air, on the MIL-7024 C-type II calibrating fluid that was used for all testing. This data sequence is representative of the operational stability and performance level of this particular device and, more generally, of all 254  $\mu\text{m}$  orifice diameter SPRAY TRIODE® devices.



### Aerometrics LDPA/SPRAY TRIODE® Test Chamber Experiments:

The photograph of Figure II-23 provides an overall view of the manner in which the test chamber was positioned with respect to the Aerometrics LDPA and the SPRAY TRIODE® Test system. As can be seen the LDPA laser, mounted on the bench to the right, was positioned so as to project the probe beam through one of the two diametrically opposed viewports. For all testing the probe beam volume was positioned 133 mm above the aluminum mat on the chamber bottom. The receiver unit to the left was placed so as to permit of this probe volume through the 45° off axis viewport, although the resolution of the photograph is too low to permit the electrical and gas lines to be seen, all were directly connected to the existing SPRAY TRIODE® test system.

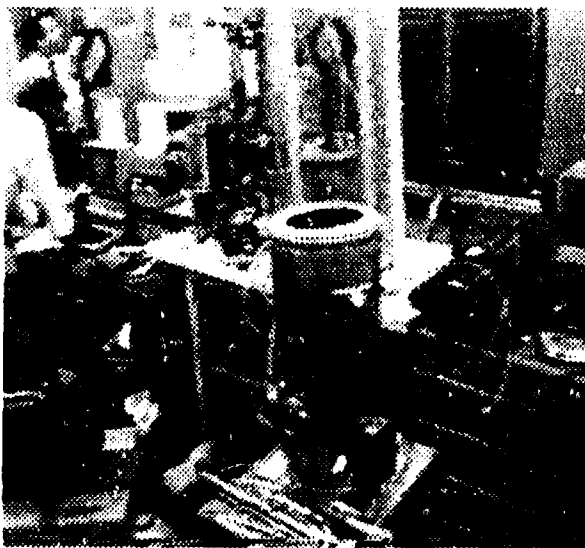


Figure II-23

As a point of reference, the rectangular object below the white bench and between the test chamber the receiver and the test chamber is the electronics control box of the Nichols-Zenith pumping station. The LDPA computer system that is shown in Figure II-24 was mounted close to the SPRAY TRIODE® computer to facilitate data collection.



Figure II-24

### III. RESULTS

#### Atmospheric Testing:

In order to develop a data base that will be suitable for the general characterization of SPRAY TRIODE® plumes under atmospheric (nitrogen) conditions, a series of lateral surveys were obtained 10 cm and 20 cm downstream of the orifice. Each lateral survey included data collection on the centerline, and at positions 2 cm, 4 cm, and 5 cm radially outward from the centerline, with the plume centerline aligned parallel with the test chamber axis. Geometrical constraints prevented data from being obtained at lateral positions beyond 5 cm.

A wealth of observational data has established that the plume can be generally characterized as having a two regime structure consisting of an inner large droplet core zone and an outer small droplet sheath region. The inner core zone corresponds to the large droplet portion of the global (Malvern and theoretically predicted) distribution (cf Figure I-3), whereas the sheath region relates to the portion of the global distribution residing to the small droplet side of the prominent peak.

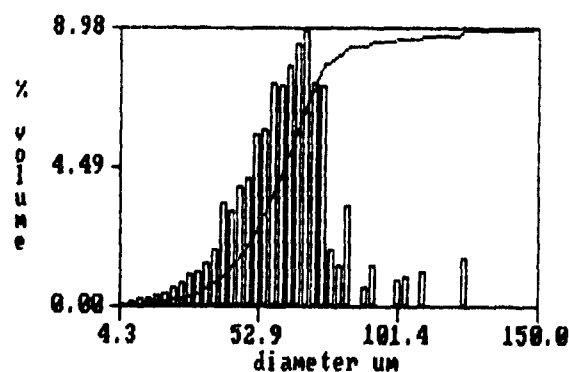


Figure III-1

Figure III-1 obtained at a position 10 cm down, and 5 cm laterally from the centerline during operation at 1.1 bar (absolute), a mean charge density level of  $1.4 \pm 10\%$  C/m<sup>3</sup>, and a flow rate of 1.14 mL/sec exemplifies the type of spray droplet distribution that exists in the sheath zone close to the core/sheath boundary region. This distribution has a Sauter mean diameter ( $D_{3,2}$ ) of 56.3  $\mu$ m, a span of 0.7 and 10% and 90% points of 37.0  $\mu$ m and 78.6  $\mu$ m respectively. The precipitous, large droplet cutoff, in this instance at approximately 80  $\mu$ m, is a general feature of SPRAY TRIODE® plumes.

A small droplet cut off at about 15 to 20  $\mu$ m, is also a characteristic of these sprays but is masked in these data by droplet impact atomization. This secondary haze generation accounts for the small droplet peak (cf. the corresponding number distribution of Figure III-2) and for the low number median size of 19.0  $\mu$ m. Note, that with the exception of this small droplet peak, the number distribution is almost uniform. The small population of large droplets larger than  $\approx 80 \mu$ m is a consistent feature

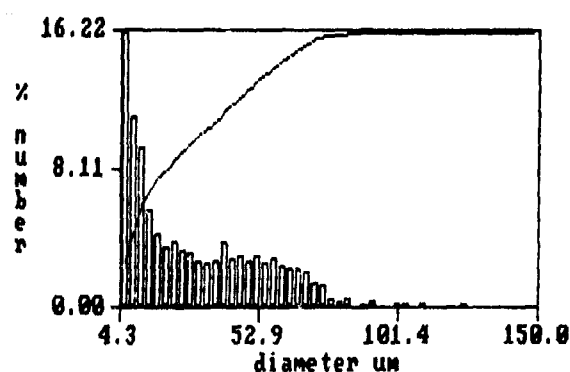


Figure III-2

of all of the measurements made to date. Velocity measurements show that these droplets originate either as drippings of spray fluid that is collected in the vicinity of the sprayer, or are droplets formed by entrainment of the collected fluid that drains along the sprayer toward the orifice. Both sources would obviously be radically reduced in the presence of a modest (several meters/sec) external flow field.

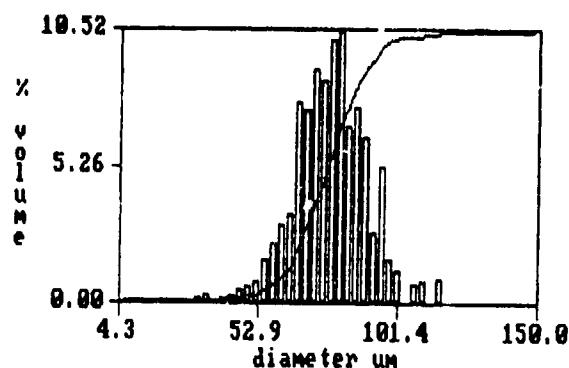


Figure III-3

The volume size data of Figure III-3 were obtained under comparable operating conditions to those prevailing for Figure III-1, ( $1.5 \pm 10\%$  C/m<sup>3</sup>, 1.07 mL/sec, 1.0 bar) and at the same vertical distance from the orifice, but sufficiently close to the orifice (4 cm rather than the 5 cm) to intercept the fringe of the large droplet core. Although the span of this distribution (0.4) is somewhat smaller than that observed at the 5 cm lateral position, and the distribution is well confined to 10% and 90% points of 60.8 and 93.5  $\mu\text{m}$  respectively, the 75.8  $\mu\text{m}$  Sauter diameter of this distribution is markedly larger than the 56.3  $\mu\text{m}$  value at the 5 cm position. Again, there is a small and sparse population of larger droplets ( $\approx 115 \mu\text{m}$ ) beyond the nominal end of the distribution at  $\approx 100 \mu\text{m}$ . It is noteworthy that there is no meaningful volume of droplets having sizes below  $\approx 50 \mu\text{m}$ ; a feature that, along with the generally well defined and abrupt large drop-

let margin, and the abbreviated small droplet "tail", are innate characteristics of all electrostatic sprays generated by direct charge injection.

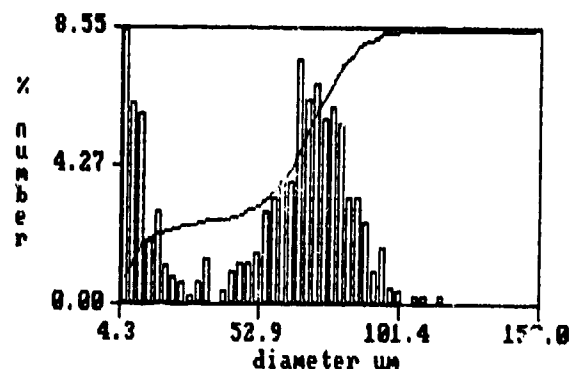


Figure III-4

While the volume fraction of small droplets having sizes of 50  $\mu\text{m}$  or below is miniscule, the number distribution data for this run, displayed in Figure III-4, reveals the existence of a well defined small droplet population below about 30  $\mu\text{m}$ , a population that increases with decreasing size. This population, as noted previously, is attributed to secondary impact atomization of the vigorously dispersed spray droplets as they encounter the chamber walls.

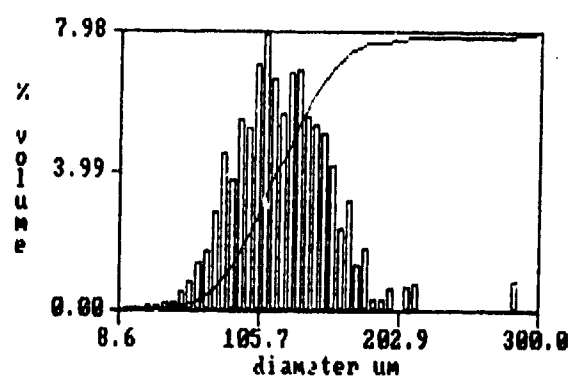


Figure III-5

The core region is exemplified by the volume size data of Figure III-5, which were obtained at the same 10 cm vertical position but at only 2 cm from the plume centerline. These data

were obtained during operation at about the same charge density level ( $1.5 \pm 10\%$  C/m<sup>2</sup>) but a somewhat lower flow rate (0.84 mL/sec) than were the previous examples. The span of this distribution is 0.7 with 10% and 90% points of 74.0 and 157.3  $\mu\text{m}$ , respectively; values that are substantially larger than those encountered in regions outside the core zone.

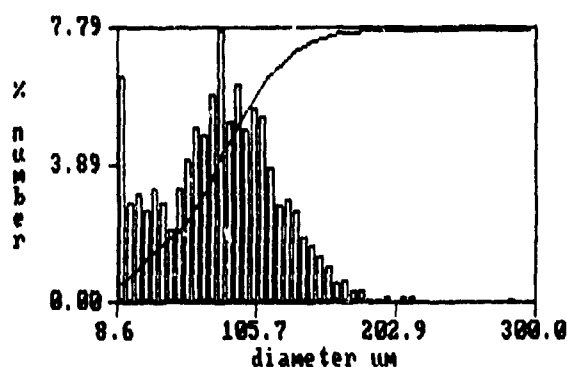


Figure III-6

These larger values are, of course, reflected by the Sauter mean diameter, which is now 111.8  $\mu\text{m}$  (compare this to the predicted size distribution of figure I-3). The number distribution data of Figure III-6 shows that there is a meaningful droplet population beyond 100  $\mu\text{m}$  and an even larger population of smaller droplets. Again the bimodality of the distribution is well defined, with the second small droplet population confined to  $\approx 50$   $\mu\text{m}$  and below. In addition, the data of Figures III-5 and 6 both exhibit large droplet tails that are uncharacteristically long for charged spray distributions. These tails are attributed to entrainment and subsequent atomization of fluid that has collected on the spray head and drained downward to the orifice of the vertically downward pointed device. This mechanism, plus liquid dripping from the support structure, is, as previously noted, considered to be responsible for the small population of 200 to 300  $\mu\text{m}$  droplets that are a feature of most distributions obtained to date.

These data, and a comparable set that was obtained at 20 cm from the orifice, confirm the expectation that the droplet sizes are in quantitative agreement with theoretical predictions (cf Figure I-3).

#### Pressure Effects:

An extensive data base has been developed concerning the influence of background conditions upon output charge density level, and overall operational behavior of SPRAY TRIODE® devices. These data demonstrate, beyond question, that conditions in the immediate vicinity of the orifice exit influences attainable output charge density level and the resultant droplet development process. The mechanism underlying this interaction is easy to understand. The SPRAY TRIODE® device, as previously noted, is functionally the same as a Van de Graaff generator insofar as modest ( $\approx 10$  kV) input voltages are capable of producing exiting streams with surface electric field strengths of upwards of 13 MV/m. This field strength, which is associated with maximal charge injection, with almost uniform charging of the exiting stream and with the small droplet sizes and narrowest droplet distributions (cf Figure I-6), are clearly well in excess of the 3 to 4 MV/m breakdown strength of atmospheric air. It is important to note that since the breakdown strength of atmospheric pressure nitrogen is somewhat lower than that of air (due to the absence of the protective effects of electronegative oxygen) performance in this test gas will be slightly degraded compared that measured in air.

The droplet development process occurs within the first few millimeters of the orifice, consequently substantial increases in output charge density level can be achieved by protecting this critical region from the debilitating effects of corona breakdown. This is most easily

accomplished by surrounding the exiting stream with a high breakdown strength atmosphere that extends to the point where the drop-formation process is complete. Once the jet has formed corona effects are no longer of importance. The presence of high breakdown strength gases such as  $\text{SF}_6$ , Freon and most hydrocarbon vapors in the vicinity of the exit plane will effectively forestall the corona breakdown process and will permit the attainment of column field strengths and output charge density levels well in excess of those that are achievable in the absence of corona suppression measures. Such increases in output charge density level are accompanied by equally dramatic visual changes in the plume structure. The spray becomes more vigorous and, most importantly, is visually more uniform and finer. The distinct large droplet core shrinks and merges with the small droplet sheath when corona suppression is applied.

The use of high breakdown strength blanketing gas provides a vivid demonstration of the theoretically expected behavior. The minimum energy model of SPRAY TRIODE® performance (8,9) shows the existence of a direct relationship between the electric field strength at the surface of the exiting stream, the uniformity of the charge density radial profile of the exiting column, the maximization of total output charge density level, and the generation of narrow droplet distributions having minimal sizes.

All SPRAY TRIODE® performance data, obtained to date, correlate well with breakdown electric field strengths calculated using the orifice size as a measure of the stream dimension. Consequently, it is reasonable to use this dimension as the characteristic length parameter ( $d$ ) for the estimation of the Paschen Pd parameter and for the evaluation of the manner in which breakdown strength varies

with background pressure. At atmospheric pressure, the 254  $\mu\text{m}$  orifice dimension of the device used for all testing has a Pd value of  $\approx 20$ . This is sufficiently above the Paschen minimum for air and nitrogen (20) to assure that breakdown strength will be almost linearly related to pressure. The theoretical droplet distributions of Figures I-3 to I-6 are based on this observation.

The data that have been obtained during operation at elevated pressure are inconsistent with this model of SPRAY TRIODE® behavior. Figures III-7 to III-13 display droplet volume distributions that were obtained at various background pressures (1.9, 3.0, 3.5, 4.3, 4.9, 5.3, and 5.9 bar absolute) with the probe volume positioned 10 cm downward and 5 cm from the centerline. These data should be compared with the atmospheric pressure data of Figure III-1, which were obtained at the same plume position and under approximately the same operating conditions;  $1.5 \pm 12\%$  C/m<sup>3</sup> and flow rates of  $0.85 \pm 15\%$  mL/sec. A modest increase in absolute background pressure from 1.1 bar (Figure III-1) to 1.9 bar (Figure III-7) results in a proportional increase in the Sauter mean diameter (SMD) from 56.3 to 95.6  $\mu\text{m}$ .

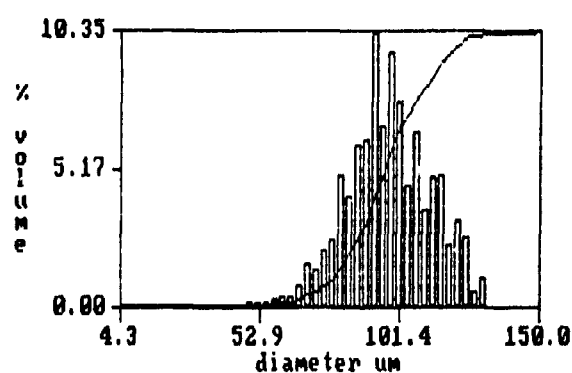


Figure III-7, (1.9 bar abs)

However, further increases in background pressure up to the 5.9 bar limit studied (Figure III-13) shows that this initial linear behavior is

soon replaced by a plateauing of SMD with pressure. Once the SMD obtains a value of  $\approx 135 \mu\text{m}$  at  $\approx 4$  bar it remains essentially unaltered as pressure is increased further. This is reflected in the output charge density level. Contrary to expectation and in contradiction to all theoretical and experimental work to date, the output charge density level remains virtually flat and independent of background conditions. From the earlier discussion, this would imply that the background gas has no effect whatever on performance, which is of course, in blatant contrast to the all blanketing gas test data that have been obtained since 1979, and using a wide variety of devices including the unit employed in these studies.

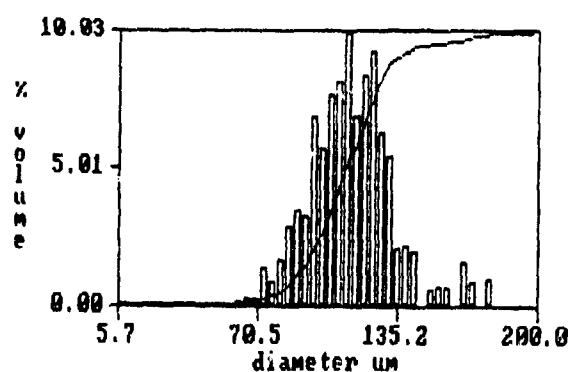


Figure III-8, (3.0 bar abs)

A clue to what is occurring can be obtained from a comparison of the droplet distributions obtained in the core region (10 cm down, 2 cm laterally, Figure III-5) and, for instance, that of Figure III-9, which was obtained at 3.5 bar absolute pressure and which has approximately the same SMD. For all intents and purposes, the data indicate that the plume is "mushrooming" with the core region expanding laterally as background pressure is increased. As a consequence, the probe volume, which is at a fixed position with respect to the orifice, and which was originally in the sheath region (under atmospheric conditions), is now measuring the core-sheath boundary. With increasing

pressure, the probe penetrates more fully into the expanded core regime until full immersion is reached at pressures of  $\approx 4$  bars and beyond. This explains why there is a plateauing of droplet size with pressure.

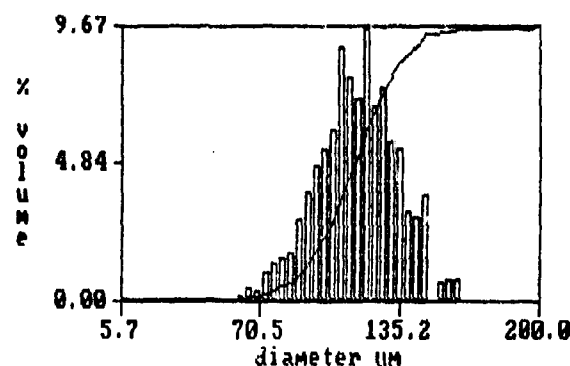


Figure III-9, (3.5 bar abs)

As shown by the theoretical plume behavior depicted in Figure I-7, plume geometry is a function of fluid dynamic, aerodynamic, and electrodynamic forces. In general lateral dispersion is due to electrostatic forces while forward penetration is a function of all three forces. There is coupling between the two velocity components as illustrated again, by the plume behavior of Figure I-7. As flow rate is increased, the forward penetrating velocity is also increased. However, there is an increased "pooling" of charge which enhances the radial electric field and, in effect, serves to make the plume self-similar. That is, the profile is preserved but displaced forward with increasing flow rate. A similar effect is occurring with plumes under the influence of increasing background pressure (density). In this instance, density effects serve to preferentially arrest droplet forward motion and to enhance radial dispersion, again due to the pooling of charge and the intensification of lateral motion.

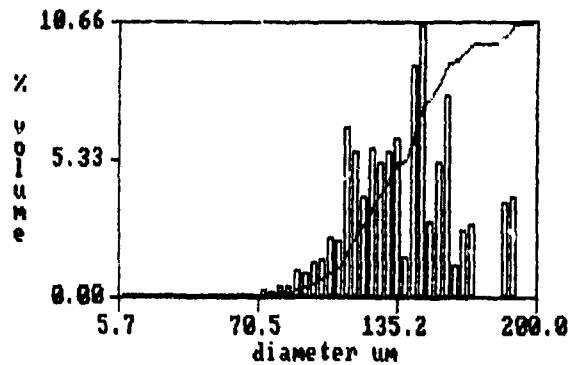


Figure III-10, (4.3 bar abs)

This scenario provides a plausible explanation for the approximate invariance of charge density level. In fact, on average, the charge density level was observed to undergo a slight decrease with pressure increase, indicating that any benefit occurring from pressure enhanced breakdown strength was counterbalanced by another effect. This effect, the presence of fluid on the spray head, has been discussed previously in the context of its influence on the droplet size distribution. In particular, collected spray fluid was implicated in the large droplet tail and the large individual droplets that are a consistent feature of all sprays studied to date. This process is also responsible for the inability of the spray devices to respond to background density increases. Under normal operating conditions, some spray fluid collection and entrainment occurs, with attendant performance loss. However, this loss, which is due to the "shorting" of the exiting column to the device exterior, is generally only on the order of 10%.

This situation is radically altered by the "mushrooming", or lateral dispersion, of the plume as pressure increases. Despite mean orifice velocities of upwards of 20 m/sec, the plume literally fills the chamber to such an extent that the elliptical end cap is wet with collected spray. This wetting occurs to a certain extent even under atmospheric condi-

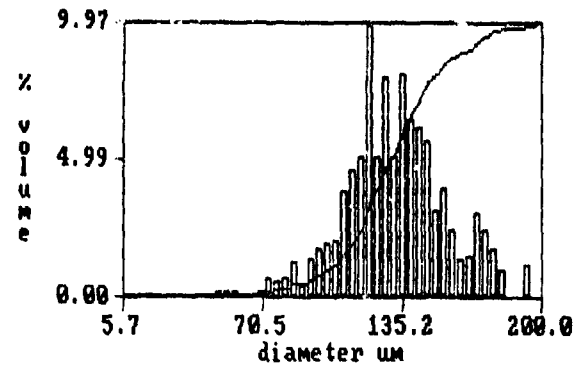


Figure III-11, (4.9 bar abs)

tions, but is most pronounced under elevated pressure conditions, a factor that attests to the vigor of charged sprays even when generated by modest charge density levels.

Compounding the entrainment produced performance diminution, is another operational factor that only became apparent when droplet sizing measurements were being made at elevated background pressures. Under normal (atmospheric) operating conditions, the spray fluid is recycled from the collector back to the spray head on a time scale that is determined by flow rate, but is roughly about 20 minutes. While the fluid is thoroughly aerated during spraying, this has never been of any consequence during operation at atmospheric conditions. However, it became immediately apparent that operation at pressures above  $\approx 1.5$  bar was aerating the fluid to the extent that performance was impaired. Sufficient gas was being introduced into the recirculated fluid to markedly reduce the dielectric breakdown strength and to limit output charge density levels to approximately half of the nominal (atmospheric) values of 1.4 to 1.6 C/m<sup>2</sup>.

Original atmospheric performance levels were recouped by allowing the fluid to stand for several hours. Once it became clear that gasification was a major contributory factor to poor high background pressure operational

performance all testing was undertaken on a once through basis with fresh, unused fluid.

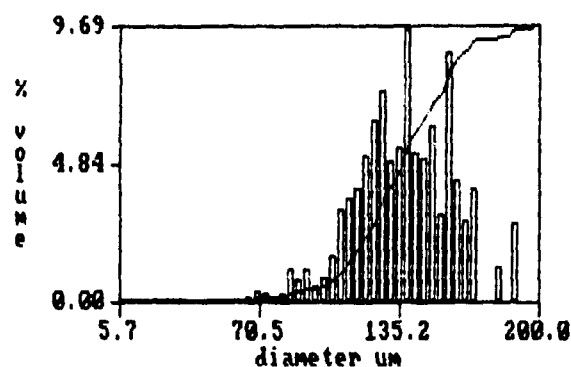


Figure III-12, (5.3 bar abs)

Both the entrainment and aeration problems are easily corrected. A positive flow of background gas can be used to alleviate collection in the vicinity of the orifice, and "once through" use of the spray fluid, as would prevail in service, will circumvent any possibility of premature, aeration induced breakdown. While straightforward, these solutions could not be properly implemented within the tight time restraints of the test program, and will have to form part of the test protocols of future such studies.

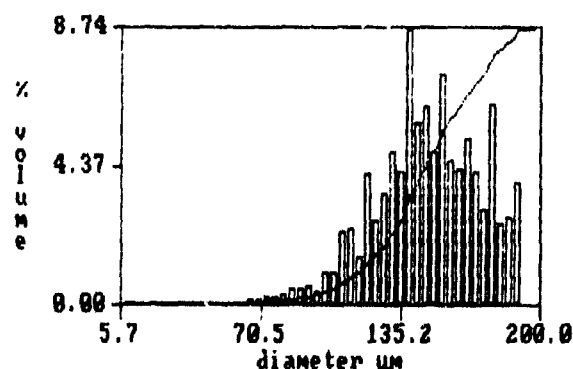


Figure III-13, (5.9 bar abs)

Despite these problems, the test data that were obtained at atmospheric pressure are in quantitative agreement with model predictions. There is no reason to suspect that the model is not also an accurate predictive tool for the description of SPRAY TRIODE® behavior at high pressure. Confirmation will have to await the results of testing with the modifications noted.



---

## IV. Potential Applications

Charge injection atomization, as exemplified by the SPRAY TRIODE® atomizer, has been demonstrated to have a number of unique attributes that recommends its use in a broad range of engine, combustion system, and other, non-fuel, related applications. By directly injecting charge into the fluid to be sprayed it is possible to create droplets in the most energy efficient manner known. Moreover, since the droplet development process is purely electrical in nature, it is decoupled from the fluid delivery process. In other words, the essential elements of the atomization mechanics are not influenced by flow rate nor, counter-intuitively, are they a function of fluid properties. A large body of experimental and theoretical evidence attests to the validity of these attributes. Most importantly, as indicated by theory, and as verified by the tests conducted during the course of this work, charge injection atomization produce highly dispersive droplet sprays having droplet sizes that are in a range of interest for combustion, painting, baking, and agricultural spraying, plus other applications such as oil mist lubrication and ultrafiltration.

In its current state of development this method of atomization is best suited for use with electrically insulating fluids such as fuels, vegetable oils, lubricating oils, pharmaceutical and cosmetic oils. Of all the potential applications perhaps the most appropriate will be in gas turbine fuel systems. The ability to provide a uniform, dispersive spray without the need for

a large power expenditure and external aerodynamic or fluid mechanical assistance when flowing fuels of varying viscosity and density would greatly benefit the design of these systems and engine performance in general. However, existing SPRAY TRIODE® designs involve the use of small orifice sizes (1/4 mm is typical), and although it is possible to use shower head orifice and slit arrays increase flow rate capability, initial designs will necessarily have low to modest flow rate capability. This does not represent an inherent limitation of the charge injection atomization, concept, but rather it is representative of the particular device design now in use. Alternate designs can overcome this limitation but at the expense of a longer development effort to first application.

Consequently, the first use should be in low flow rate applications such as small gas turbine fuel systems and as part of the ignitor systems for both small and medium sized engines. This latter application is particularly intriguing insofar as SPRAY TRIODE® devices can provide vigorous, energy efficient spraying under the adverse conditions that are commonly encountered during relight at altitude. Whether the sheath droplet volume/size distributions exemplified by Figures III-1,2 are adequate for this service or much finer, and more highly charged dispersive sprays will be have to be generated is not known at this time. Such matters will have to form part of a future evaluation of this technology.

---

## V. REFERENCES

1. Kelly, A.J., "Electrostatic Atomization Device", US Patent No. 4,255,777, March 1981.
2. Kelly, A.J., "The Electrostatic Atomization of Hydrocarbons", *Journal Inst. Energy*, 312, June, 1984.
3. Kelly, A.J., "Electrostatic Metallic Spray Theory", *JAP* 47, (121), 5264, 1976.
4. Kelly, A.J., "Electrostatic Spray Theory", *JAP* 49, (5), 2821, 1978.
5. Kelly, A.J., "Low Charge Density Electrostatic Atomization", *IEEE/IAS Transactions*, IA-20, 267, 1984.
6. Simmons, H.C., Kelly, A.J., "Electrostatic Spraying of Oil-Based Agricultural Products", *Pesticide Formulations and Applications Systems: Fifth Volume*, ASTM STP 915, L. D. Spicer and T.M. Kaneko, Eds., American Society for Testing and Materials, Philadelphia, 1986, pp. 56-64.
7. Simmons, H.C., Kelly, A.J., "SPRAY TRIODE Electrostatic Agricultural Atomizer: Development Update", *Pesticide Formulations and Applications: Sixth Volume*, ASTM STP 943, D.I.B. Vander Hooven and L.D. Spicer, Eds., American Society for Testing and Materials, Philadelphia, 1987, pp. 88-100.
8. Kelly, A.J., "Charge Injection Electrostatic Atomization: Modeling I", American Association of Aerosol Research paper No. 15B, 1987 Annual Meeting of AAAR, University of Washington, Seattle, Washington, September, 1987.
9. Kelly, A.J., "Charge Injection Electrostatic Atomizer Performance Modeling", proceedings of the 4th International Conference on Liquid Atomization and Spray Systems, Sendai, Japan, August 1988.
10. Lue, K-M, Kelly, A.J., "Quadrupole Mass Spectrometer Measurements of Electrostatic Sprays", *Electrostatics 1987 Institute of Physics Conference Series number 85*. Ed. J.L. Sproston, Institute of Physics, Bristol and Philadelphia, 337, April 1987.
11. Harstad, K., Bellan, J., "Electrostatic Dispersion of Drops in Clusters", accepted for publication in *Combustion Science and Technology*, 1989.
12. Bankston, C.P., Back, L.H., Kwack, E.Y., Kelly, A.J., "Experimental Investigation of Electrostatic Dispersion and Combustion of Diesel Fuel Jets", *ASME J. Eng. Gas Turbine and Power*, 110, 361, 1988.
13. Miller, J.A., Biblarz, O., Zajdman, A., Manning II, W.W., Marvoudis, J.A., "Electrostatic Spray modification in Gas Turbine Combustion", *AIAA J. Propulsion*, 1, 187, 1987.
14. Zajdman, A., "Electrical Spray Modification With Various Fuels In A T56 Combustor", contractor report NPS-67-83-003CR, Naval Postgraduate School, Monterey, CA. 1984.
15. True, M., "Modeling of Electrostatic Spray Plumes", *IEEE/IAS Transactions*, IA-19, 754, 1983.
16. Bellan, J., "A New Approach To Soot Control In Diesel Engines By Fuel Drop Charging", *Combustion and Flame*, 51, 117, 1983.
17. Bachalo, W.D., Houser, M.J., "Phase/Doppler Spray Analyzer For Simultaneous Measurements Of Drop Size And Velocity Distributions", *Optical Engineering* 23, 583, 1984.
18. Bachalo, W.D., Rudoff, R.C., Brena de la Rosa, "Mass Flux Measurements Of A High Number Density Spray System Using The

Phase Doppler Particle Analyzer", AIAA #88-0236, AIAA 26th. Aerospace Science Meeting, Reno, N.V., January 11, 1988.

19. Bachalo, W.D., Brena de la Rosa, A., Rudoff, R.C., "Diagnostics Development For Spray Characterization In Complex Turbulent Flows", ASME #88-GT-241, Gas Turbine And Aeroengine Congress Amsterdam, ND, June 6, 1988.

20. Marode, E., "The Glow To Arc Transition" in Electrical Breakdown And Discharges In Gases: Macroscopic Processes And Discharges, Edited by Erich E. Kunhardt and Lawrence H. Luessen. NATO ASI Series, Series B: Physics, Vol. 896 pp. 119-166, Plenum Press, (1983).

---

## VI. APPENDIX

### SBIR TEST CHAMBER MECHANICAL DRAWINGS

PAGE VI-2: Top View of Ports and Support Rod Mounting Hole Geometry

PAGE VI-3: Top Closure Lid Design

PAGE VI-4: Upper Rod Cage Support Plate Design

PAGE VI-5: Bottom Closure Plate Design

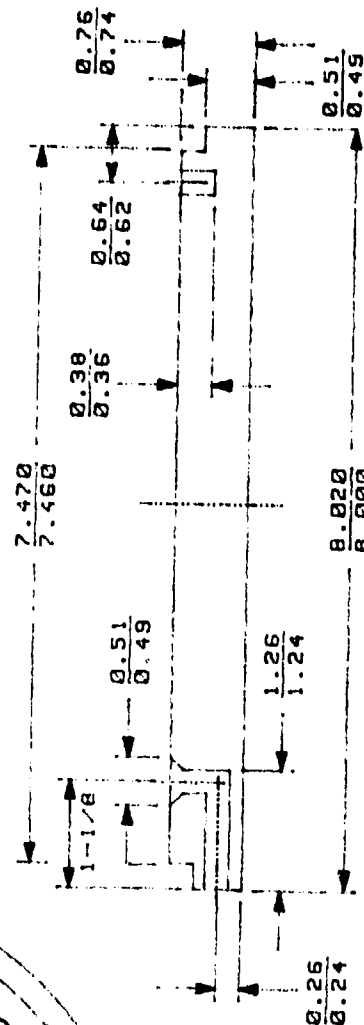
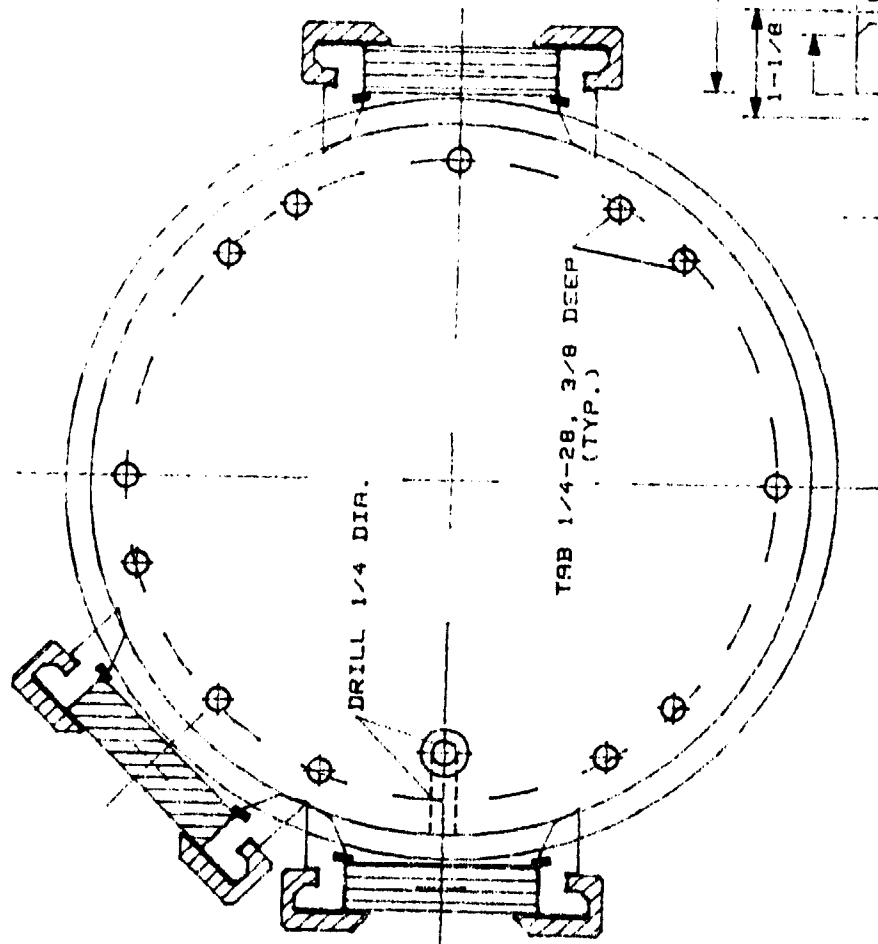
PAGE VI-6: Viewport Assembly Drawing

PAGE VI-7: Viewport Body Design

PAGE VI-8: Viewport Split Support Ring Design

PAGE VI-9: Viewport Split Ring Retainer Design

MATERIAL: ASTM ALUMINUM



SCALE 1:2

UNIT: INCHES

SECTION A-A

SUBJECT: SBIR TEST CHAMBER -  
PORTS/ROD HOLE LOCATIONS

SBIRPORT

ZYW

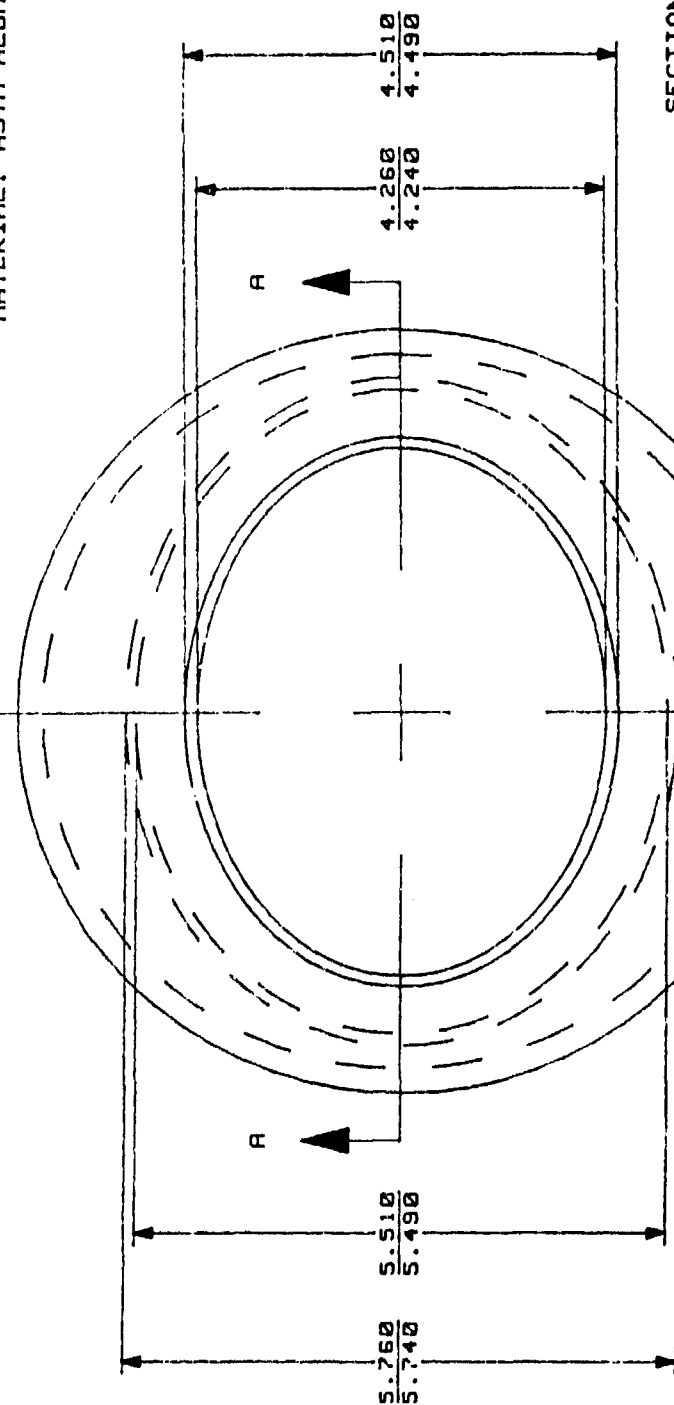
REV.

ZYW CORP.  
P.O. BOX 279  
PRINCETON JCT., NJ 08550 USA

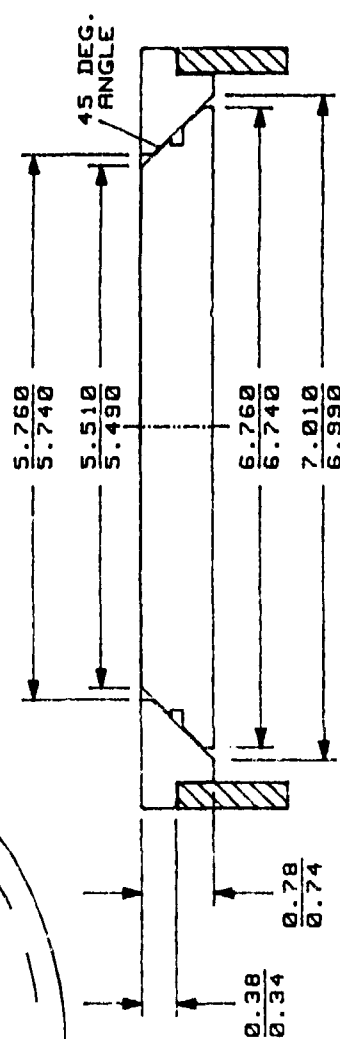
A

REV.	DATE	BY	ISSUED FOR
A	10/03/89	SLK	PROTOTYPE

MATERIAL: ASTM ALUMINUM



SECTION A-A



SCALE 1:2

UNIT: INCHES

SUBJECT: SBIR TEST CHAMBER -  
TOP LID

SBIRTLID

⑤

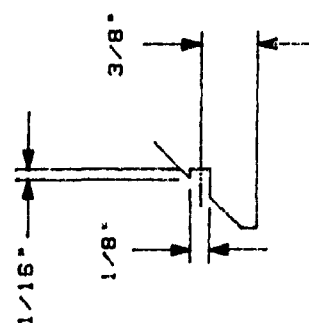
REV.	DATE	BY	ISSUED FOR
A	10/27/89	SLK	PROTOTYPE

ZYW

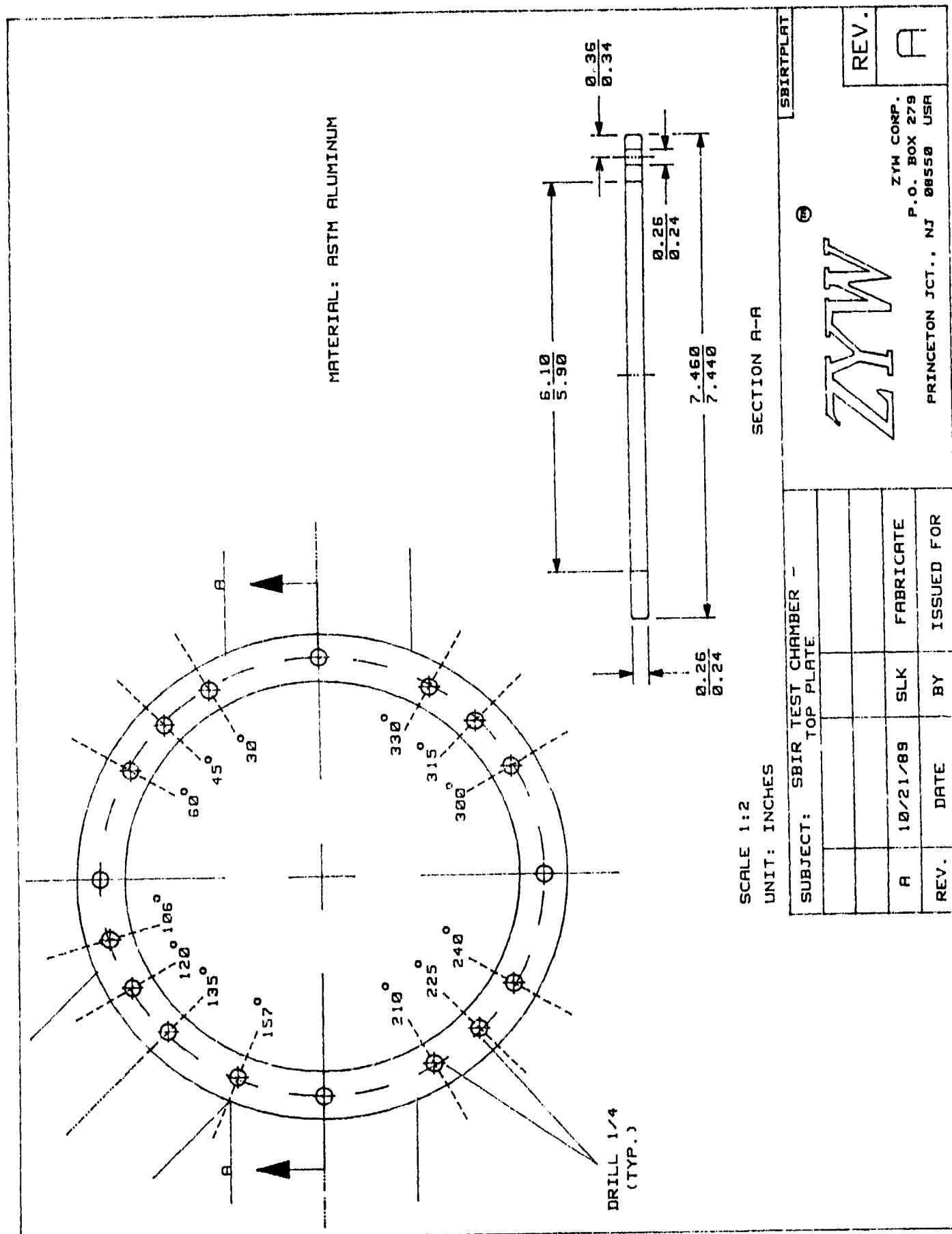
ZYW CORP.  
P.O. BOX 278  
PRINCETON JCT., NJ 08550 USA

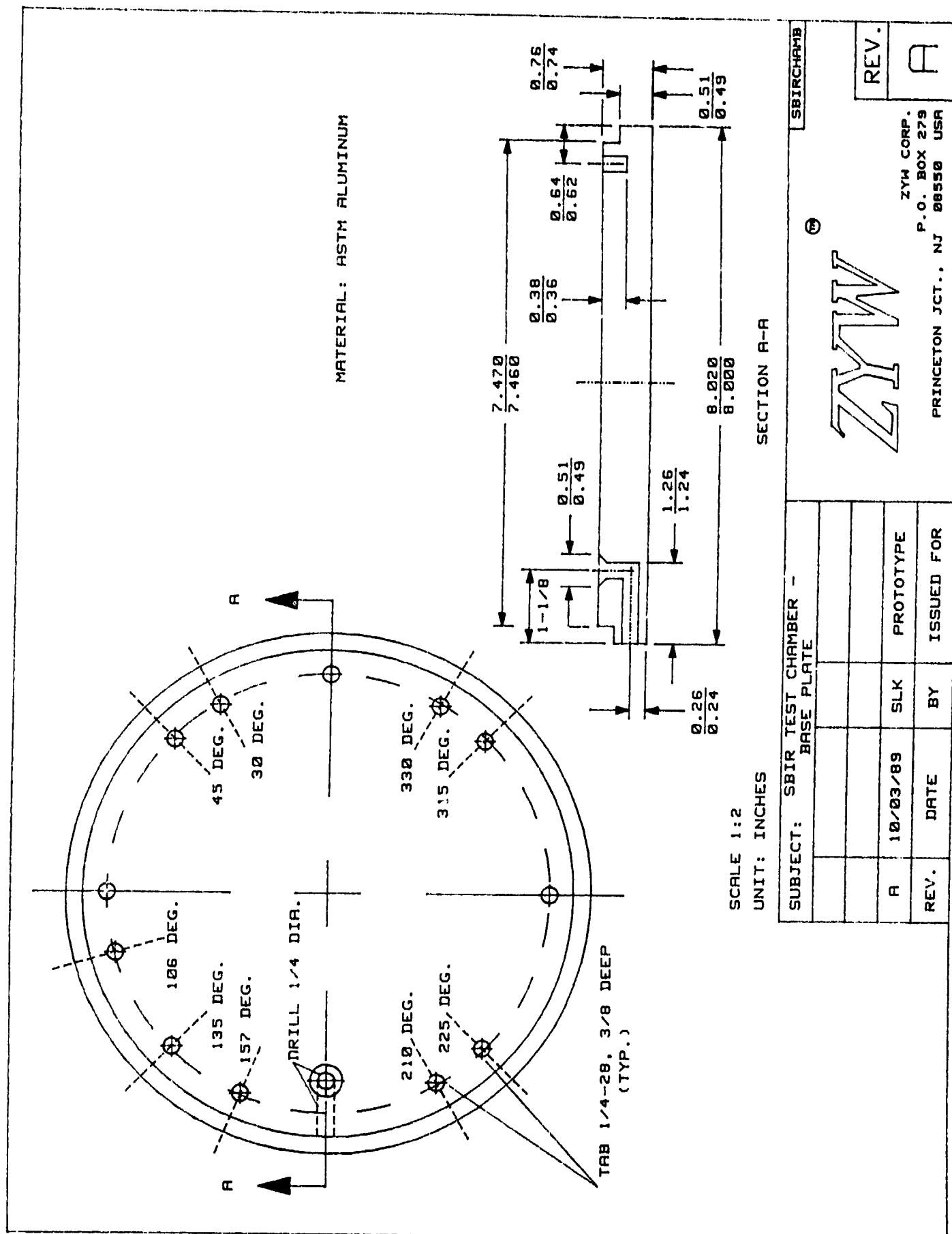
REV.

A

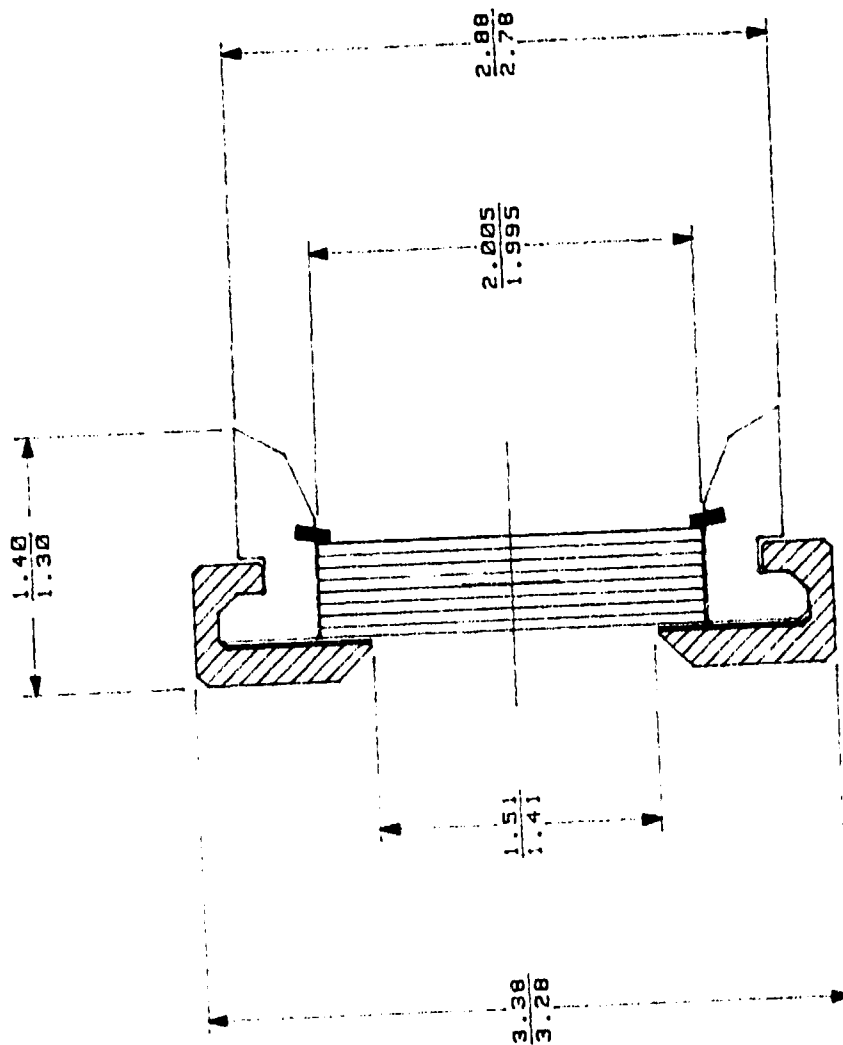


O' RING  
GROOVE DETAIL  
(NTS)









SCALE 1:1

ALL UNITS IN INCHES

SUBJECT: SBIR TEST CHAMBER PORT  
DETAIL

REV.	DATE	BY	ISSUED FOR
B	10/12/89	SLK	REVISED SPLIT RING
A	10/10/89	SLK	DOCUMENTATION

SBIRPORTA

ZYW

REV.

ZYW CORP.  
P.O. BOX 278  
PRINCETON JCT., NJ 08550 USA

B

